the crossover.

These two competing mechanisms lead to an optimum in the crossed parts of Fig. 3, which is in reasonable agreement with the a and b peaks of the data.

To this discussion we have to add the density of states. In the weak-coupling limit the two branches contribute equally, but in the strong-coupling region (θ large, $\perp$ polarization) the lower branch is much favored.

The authors express their appreciation to Mr. Moulin of Thompson C.S.F. for providing the very pure samples of CdS.

*Laboratoire associé au Centre National de la Recherche Scientifique.

[1]J. J. Hopfield, Phys. Rev. 112, 1555 (1958).
[2]J. J. Hopfield and D. G. Thomas, J. Phys. Chem. Solids 12, 276 (1960).
[3]J. J. Hopfield and D. G. Thomas, Phys. Rev. 122, 35 (1961).
[4]J. J. Hopfield and D. G. Thomas, Phys. Rev. Letters 15, 22 (1965).
[5]E. Gross, S. Permogorov, and B. Razbirin, J. Phys. Chem. Solids 27, 1647 (1966).
[6]C. Benoit a la Guillaume, J. M. Debever, and F. Salvan, Phys. Rev. 177, 567 (1969).
[7]D. C. Reynolds, R. N. Euwema, and T. C. Collins, in *Proceedings of the Ninth International Conference on the Physics of Semiconductors, Moscow, U. S. S. R., 1968* (Nauka, Leningrad, U.S.S.R., 1968).
[8]J. J. Hopfield, J. Phys. Soc. Japan Suppl. 21, 77 (1966).
[9]G. D. Mahan and J. J. Hopfield, Phys. Rev. 135, 428 (1964).

TWO-BAND ELECTRON-PHONON INTERACTION IN RHENIUM*

D. A. Robinson and M. Levy
Department of Physics, University of California, Los Angeles, California 90024
(Received 6 April 1970)

Anomalies were observed in the electronic component of the ultrasonic attenuation of transverse and longitudinal waves in high-purity rhenium, which could not satisfactorily be explained by the free-electron or real-metal theories of Pippard. A two-band model will be developed to explain the observed attenuation.

Many features of the electron-phonon interaction in metals can be explained by treating the electron system in the free-electron approximation.[1] Included is the prediction of a maximum in the ultrasonic attenuation of transverse waves for sufficiently high frequencies (about 10^9 sec^{-1}) and for $ql > 1$, where $\vec{q}$ is the impressed phonon wave vector and l is the electron mean-free path. At these frequencies the forces arising from electromagnetic coupling start to vanish and only those forces arising from collision drag remain. The maximum appears to be associated with the collision drag term and occurs for a ql value of about 2. For longitudinal waves such an effect is not predicted up to frequencies of the order of the plasma frequency (about 10^{15} sec^{-1}). Further refinements in the theory such as the inclusion of a deformation potential have led to better agreement between experiment and theory, but have not predicted additional anomalies in the ultrasonic attenuation in metals for ql on the order of 1.[2,3]

We have observed a maximum in the attenuation of transverse waves in rhenium as a function of temperature, but at frequencies an order of magnitude lower than predicted. Also, and perhaps most important, a maximum was observed in the longitudinal attenuation[4] which appeared to occur at roughly the same ql value as for the transverse waves. The two-band model to be developed below is proposed to explain this anomaly since our attempts to fit the observed attenuation to available free-electron and real-metal theories were not entirely successful.

The sample on which the measurements were taken is a rhenium single crystal 0.627 cm long by about $\frac{1}{2}$-cm diam, with a resistivity ratio in excess of 30 000. The sample ends were spark cut, polished, and etched, with crystal orientation along the [0001] axis to better than ±1°. A cadmium sulfide thin-film transducer with a shear fundamental of 200 MHz was deposited on one end.

Ultrasonic measurements were made at frequencies from 130 to 600 MHz by the pulse-echo technique, using a Matec attenuation comparator and attenuation recorder. All measurements were made for $\vec{q} \| [0001]$ direction. The estimated accuracy of the attenuation measurements is about ±2%. The temperature dependence of the attenuation coefficient was measured from 60°K to less than 0.5°K. Using a calibrated Ge resis-

tance thermometer from Cryocal, temperature measurements were made with a PAR HR-8 lock-in amplifier at 37 Hz. The estimated accuracy of measurement is about ±1% for temperatures above 1°K. Attenuation versus resistance was recorded continuously on a Mosely X-Y plotter. Temperatures to below 0.5°K were obtained using a He^3 cryostat. To minimize temperature gradients between resistor and sample, He^3 transfer gas, at about $\frac{1}{2}$ atmosphere STP, was sealed in the sample chamber.

Rhenium is superconducting below 1.69°K, and the attenuation in the superconducting state below 0.5°K was used to establish the level of non-electron-phonon contribution to the attenuation. Figure 1 shows the experimental attenuation in rhenium as a function of temperature; the solid line shows the two-band theoretical fit. The poor fit at the high temperatures is to be expected since the temperature-dependent attenuation due to dislocation damping has not been subtracted from the total attenuation; it is assumed, however, that this contribution is negligible in the region of interest.[5]

Before developing the theory it should be remarked that rhenium has a rather complicated Fermi surface consisting of at least five sheets[6] —of which one hole sheet and one electron sheet of nearly equal volumes in k space account for about 95% of the total carrier concentration. Rhenium has two atoms per unit cell; thus one would expect the total volumes in k space of holes and electrons to be equal. However, the manner in which these carriers contribute to various phenomena depends not only on such parameters as effective masses and relaxation times at the Fermi surface, but also on whether the sheets in the extended zone are open or closed. In particular, in the case of rhenium, the electron sheet is roughly cylindrical and is open along the [0001] direction, while the hole sheets are roughly ellipsoidal and closed. Thus, one would expect the ratio of the effective number of electrons to holes to be less for motion $\parallel$[0001] direction than for motion $\perp$[0001]. This fact will be used later when values of the two-band-model parameters are chosen for the transverse-wave attenuation and for the longitudinal-wave attenuation.

For our two-band model, we will assume closed spherical electron and hole surfaces, differing in general in effective numbers of carriers, in effective masses, and in relaxation times. Interband transitions and deformation potential effects will be neglected for the present. We believe that the essential features of our ultrasonic attenuation data can be explained without invoking these complications.

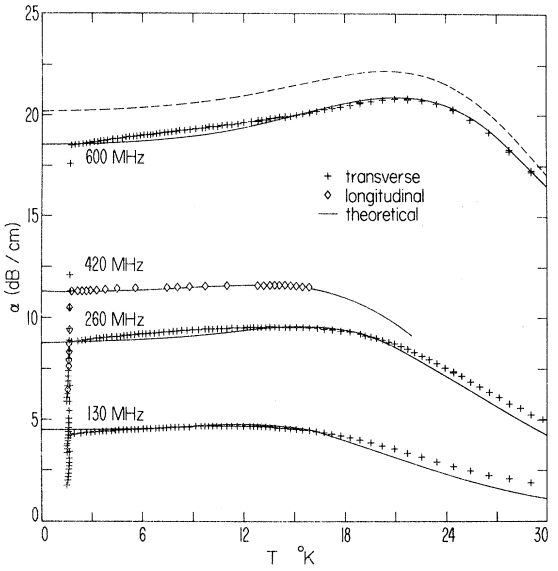

FIG. 1. Comparison of measured ultrasonic attenuation versus temperature in rhenium for $\vec{q}\parallel$[0001] direction with the two-band theory. The solid curves are the theoretical best fits to the data, including incomplete screening effects for the transverse waves. The dashed curve shows the theoretical attenuation for transverse waves if complete screening is assumed; at 260 and 130 MHz the dashed and solid curves overlie each other.

Holstein[7] has shown that for a general Fermi surface the mean velocity of the electrons associated with ultrasonic absorption due to collision drag is given by

$$\langle \vec{v} \rangle_{av}^{(1)} = \vec{u} \cdot \langle m/\underline{m}_k^* \rangle_{av},$$

where $1/\underline{m}_k^*$ is the reciprocal mass tensor, m is the free electron mass, and $\vec{u}$ is the impressed lattice velocity.

Using an approach similar to one described in Bhatia,[5] the above result of Holstein implies that for a single spherical Fermi surface of effective mass m_e the rate at which electrons per unit volume lose their energy irreversibly to the lattice is given by

$$Q = -\langle (4\pi^3)^{-1} \int \tfrac{1}{2} m_e [\vec{v}_k - (\vec{u} m/m_e)]^2 \times (\partial f/\partial t)_{coll} d^3k \rangle_{\text{Avg over cycle}}$$

with $(\partial f/\partial t)_{coll} = -(f - \bar{f})/\tau$ in the relaxation-time approximation, where $f = f(\vec{x}, \vec{k}, t)$ is the Fermi distribution function, τ is the relaxation time,

and $\bar{f} = f_0([\vec{k} - m\vec{u}(\vec{x}, t)/\hbar], \epsilon_F(\vec{x}, t))$ is the locally relaxed Fermi distribution function, and ϵ_F is the local Fermi energy. Notice that $\vec{u}m/m_e$ rather than $\vec{u}$ appears in the equation; that is, the component of electron velocity associated with ultrasonic absorption appears to relax to a mean velocity given by $\vec{u}m/m_e$ rather than $\vec{u}$. However, Holstein further shows that there is also an induced component of electron velocity given by

$$\langle \vec{v} \rangle_{av}^{(2)} = \vec{u} - \langle \vec{v} \rangle_{av}^{(1)}$$

which responds essentially instantaneously to the lattice and which, even though it does not play a direct role in ultrasonic absorption, must be taken into account in determining the total current due to the electrons and ions.

By straightforward calculation using the usual definition of electronic current and the Boltzmann equation in the relaxation-time approximation, one finds, neglecting powers of $\vec{u}$ higher than the second, the power absorption per unit volume to be

$$Q = \tfrac{1}{2}\,\mathrm{Re}\{\vec{J}^* \cdot \vec{E} - (m\vec{u}^*/\tau) \cdot [\vec{J}/(-e) - (n\vec{u}m/m_e)]\},$$

where the asterisks denote complex conjugates, $\vec{J}$ is the electronic current, $\vec{E}$ is the electric field, e is the (positive) electron charge, and n is the electron density. Note how the effective mass appears in the second term of the equation.

Ultrasonic absorption by a spherical hole surface can be found by simply changing the sign of the charge in the equations for absorption by a spherical electron surface, and otherwise treating the effective mass as positive.[8]

When both electron and hole surfaces are considered together, again by straightforward calculation using the appropriate definitions of currents and distribution functions for electrons and holes (the electric field is the same for both bands), and emphasizing again that there are no interband transitions, one finds the power absorption per unit volume in the two-band model to be

$$Q = \tfrac{1}{2}\,\mathrm{Re}\{(\vec{J}_e^* + \vec{J}_h^*) \cdot \vec{E} - (m\vec{u}/\tau_e) \cdot [\vec{J}_e/(-e) - (n_e\vec{u}m/m_e)] - (m\vec{u}^*/\tau_h) \cdot [(\vec{J}_h/e) - (n_h\vec{u}m/m_h)]\},$$

where the subscripts e and h refer to the electrons and holes, respectively. We also find, using the definitions of transverse and longitudinal electric fields in terms of the electronic and ionic currents (including the ionic current, the instantaneously induced electronic current of Holstein), and neglecting $\omega\tau$ compared to 1,[9,5] where ω is the impressed sound frequency,

$$\vec{J}_{er} = \sigma_e g_{er}(\vec{E} - m\vec{u}_r/e\tau_e), \quad r = t, l, \quad \vec{J}_{hr} = \sigma_h g_{hr}(\vec{E} + m\vec{u}_r/e\tau_h), \quad \sigma_s = n_s e^2 \tau_s/m_s, \quad s = e, h,$$

$$g_{st} = (3/2a_{st}^2)[(1 + a_{st}^2)(\tan^{-1} a_{st})/a_{st} - 1], \quad g_{sl} = 3(a_{sl} - \tan^{-1} a_{sl})/a_{sl}^2 \tan^{-1} a_{sl},$$

where the subscripts t and l refer to transverse and longitudinal sound waves, respectively, σ_s is the dc electronic conductivity, and $a_{sr} = l_s q_r$.

Now the ultrasonic attenuation per unit length is given by

$$\alpha_r = 2Q/\rho c_r u_r^2, \quad r = t, l,$$

where ρ is the density and c_r is the impressed sound velocity. Using the above relations, and taking $l_e = l_h$ (a simplifying assumption which is not unreasonable when impurity or phonon scattering is dominant), one obtains again by straightforward calculation the ultrasonic attenuation per unit length

$$\alpha_r = C_r q_r \left(\frac{1 - g_r}{a_r g_r}\right) \left\{ \frac{(1 - g_r)[1 + (n_e/n_h)(m_h/m_e)^{1/2}][1 - (n_e/n_h)(m_h/m_e)]^2 X_{hr}^2}{1 + [1 + (n_e/n_h)(m_h/m_e)^{1/2}]^2 X_{hr}^2} + g_r[1 + (n_e/n_h)(m_h/m_e)^{3/2}] \right\}, \quad r = t, l,$$

where $C_r = n_h m^2 v_{Fh}/\rho m_h c_r$, $X_{ht} = g_t(4\pi\sigma_h C_t^2/C^2\omega)$, where c_t^2/c^2 has been neglected compared to 1, and $X_{hl} = g_l(\omega_{ph}^2 \tau_h/\omega)$, with $a_{er} = a_{hr} = a_r$, $g_{er} = g_{hr} = g_r$, ω_{ph} is the plasma frequency, and v_{Fh} is the hole velocity at the Fermi surface.

From the above equation it can be seen that, in the absence of additional data, in the limits of com-

plete screening ($X_{ht} \to \infty$) or complete screening breakdown ($X_{ht} \to 0$), either n_e/n_h or m_e/m_h can be chosen arbitrarily with the other parameters being adjusted accordingly. Since at present the ultrasonic frequencies are such that screening breakdown is just becoming apparent for transverse waves, it does not appear unreasonable to exercise the option of choosing either n_e/n_h or m_e/m_h in accordance with existing data on rhenium and adjusting the other parameters to give a best fit.

For transverse waves in rhenium, since there are no open surfaces $\perp$[0001] direction, as discussed previously, we may reasonably assume $n_e/n_h = 1$. Using $c_t = 2.86 \times 10^5$ cm/sec,[10,11] the values $C_t = 4.86 \times 10^{-4}$ dB, $m_e/m_h = 0.148$, and $X_{ht} = (a_t g_t/q_t^2) \times 6.80 \times 10^7$ cm^{-2} were then found to give the best fit. Magnetoacoustic and de Haas–van Alphen data[10,12] indicate the effective-mass ratio to be reasonable. The theoretical maximum in attenuation occurs for ql of about 5. It should also be noted that the electromagnetic coupling forces are starting to vanish at 600 MHz; thus, if one assumes complete screening, the dashed curve shown in Fig. 1 results for the 600-MHz attenuation while the other curves remain essentially the same.

For longitudinal waves, since there is the open electron surface $\|$[0001] direction, we chose to adjust n_e/n_h. There are no effective-mass data for the electron sheet for motion $\|$[0001] direction, but the theoretical curvature of the sheet indicates that the electron effective mass could be about as large as that of the holes; thus m_e/m_h was chosen equal to 1. With complete screening assumed ($X_{hl} \to \infty$), and using $c_l = 5.83 \times 10^5$ cm/sec,[10] the values $C_l = 9.43 \times 10^{-3}$ dB and $n_e/n_h = 0.152$ were found to give the best fit. The most important point to note is that this model does predict a maximum in the longitudinal attenuation for a suitable (and physically reasonable) choice of parameters. For the above choice of parameters the theoretical maximum occurs for ql of about 6.

To fit the theory to experiment it became necessary to assume some temperature dependence for the electron mean free path; the best fit appeared to be $l^{-1} = 1.2 \times 10^2 + 6.2 \times 10^{-1} T^2 + 2.0 \times 10^{-1} T^3 + 1.7 \times 10^{-4} T^5$. Some discussion of this is required: A recent paper has indicated that for a nonspherical Fermi surface, a T^3 dependence may dominate the mean free path in the region of interest.[13] Also, there are data to indicate that a T^2 dependence dominates at temperatures below 5°K (neglecting impurity scattering),[14] which implies that interband scattering is important in this region. This is an effect which we explicitly neglected in this model; however, since the maximum in the 600-MHz attenuation occurs above 20°K where the T^2 term is relatively unimportant, it seems reasonable to conclude that our model is still valid.

The physical explanation for the maximum in the ultrasonic attenuation is that in the one-band model, assuming complete screening, the smooth increase in the theoretical attenuation arises from a delicate complement of the collision drag force (dominant for $ql \ll 1$) with the electric force (dominant for $ql > 1$). If a second band is introduced, there is still only one electric force now to complement the collision drag forces in both bands and the balance is destroyed. The net effect is an "apparent" breakdown in the screening. However, in the two-band model, this "apparent" breakdown in screening is frequency independent, up to frequencies where real screening breakdown occurs, whereas in the one-band model the screening breakdown is quite frequency dependent.

Thus, it appears that while the inclusion of deformation potential and interband relaxation effects may be necessary to improve the fit between experiment and theory (particularly on the low-temperature, or high-ql, side of the attenuation maxima shown in Fig. 1) the two-band model described above does provide an explanation for the observed ultrasonic attenuation maximum in rhenium for both transverse and longitudinal waves.

The authors wish to express their gratitude to Professor T. Holstein for many invaluable discussions throughout the development of this theory, and in particular for his clarification of the collision drag effect.

---

*Research sponsored by the Air Force Office of Scientific Research under Grant No. AFOSR 70-1847.

[1]A. B. Pippard, Phil. Mag. 46, 1104 (1955).

[2]A. B. Pippard, Proc. Roy. Soc. (London) Ser. A 257, 165 (1960).

[3]E. I. Blount, Phys. Rev. 114, 418 (1959).

[4]H. J. Willard, Jr., Phys. Rev. 175, 367 (1968). Willard has observed a similar anomalous temperature dependence for longitudinal attenuation for $\vec{q}\|$ [0001] direction in high purity thallium.

[5]A. B. Bhatia, *Ultrasonic Absorption* (Clarendon Press, Oxford, England, 1967), Chaps. 12 and 13. It is possible that a better fit to the data may be obtained by

assuming a temperature-dependent contribution to the attenuation due to dislocation damping.

[6]L. F. Mattheiss, Phys. Rev. 151, 450 (1966).

[7]T. Holstein, Phys. Rev. 113, 479 (1959). In his article, Holstein uses $\vec{v}_i$ rather than $\vec{u}$ to denote the local impressed lattice velocity.

[8]R. A. Smith, *Wave Mechanics of Crystalline Solids* (Chapman and Hall, London, 1961), Chaps. 8-11.

[9]T. Holstein, Westinghouse Research Memo No. 60-94698-3-M17, 1956 (unpublished).

[10]L. R. Testardi and R. R. Soden, Phys. Rev. 158, 581 (1967).

[11]M. L. Shepard and J. F. Smith, J. Appl. Phys. 36, 1447 (1965).

[12]C. K. Jones and J. A. Rayne, Phys. Rev. 139, A1876 (1965).

[13]F. Carsey, R. Kagiwada, M. Levy, and K. Maki, to be published.

[14]J. T. Schriempf, J. Phys. Chem. Solids 28, 2581 (1967).

ROTATIONAL DESCRIPTION OF STATES IN CLOSED- AND NEAR-CLOSED-SHELL NUCLEI*

M. A. J. Mariscotti
Brookhaven National Laboratory, Upton, New York 11973
(Received 23 March 1970)

All ground-state bands observed in even-even nuclei, including closed-shell nuclei, are accurately predicted by a two-parameter description based on the cranking model. A hitherto unobserved discontinuity in a plot of $E(I)/E(2)$ vs $E(4)/E(2)$ is also predicted by the model.

Experimental data recently reported[1-4] appear to confirm that the gradual change of properties of ground-state bands which takes place with decreasing deformation continues well beyond the "vibrational" region and includes indeed all nuclei.[5,6] The purpose of this note is to propose a unified rotational description for all these bands based on an extension of the cranking model[7] due to Harris.[8]

In 1959 Mallmann[5] pointed out that ground-state bands in even-even nuclei (i.e., lowest excited states with spins $I=2,4,6,\cdots$ and even parity) exhibited a regular behavior when the energy ratios $E(I)/E(2)$ were plotted against $E(4)/E(2)$. The data presented by Mallmann spanned the interval

$$1 \lesssim E(4)/E(2) < 3.33. \tag{1}$$

A successful phenomenological description of these regularities in the more limited interval

$$2.23 \leq E(4)/E(2) \leq 3.33 \tag{2}$$

has been provided by the variable moment-of-inertia (VMI) model.[9] It has been shown[9] that the equations of this model are mathematically equivalent to the equations derived by Harris[8] from an extension of the cranking model[7] to the next higher order in ω^2 (ω is the angular velocity). In both approaches two parameters are involved, the moment of inertia in first order $\mathcal{I}_0$ and the coefficient C of the next-higher-order term. In (2) the upper limit corresponds to $C=0$ (the case of hard, well-deformed nuclei) while the lower limit corresponds to $\mathcal{I}_0=0$ (the case of "soft" nuclei, spherical in the ground state). In the following we discuss the solutions which are obtained when $\mathcal{I}_0$ and C are allowed to be negative.[10] We choose to follow Harris's approach because, although the solutions obtained with both models are mathematically equivalent, they are very difficult to interpret in terms of the VMI model.[11] Furthermore, since Harris's equations are derived from the cranking model,[7] one may hope to obtain $\mathcal{I}_0$ and C, which are here adjusted to fit the data, from a microscopic calculation. Such a calculation would be a valuable complement to the following analysis.

Harris's model[8] is based on the two equations

$$E_R = \tfrac{1}{2}\omega^2(\mathcal{I}_0 + 3C\omega^2) \tag{3}$$

and

$$[I(I+1)]^{1/2} = \omega(\mathcal{I}_0 + 2C\omega^2). \tag{4}$$

From Eqs. (3) and (4) one sees that, as Harris has pointed out, a different "effective" moment of inertia enters into the calculations of energy and angular momentum. It is convenient (as discussed below) to introduce a phenomenological definition of the moment of inertia $\mathfrak{I}(I)$ in terms of energy and spin as

$$E_R(I) = I(I+1)/2\mathfrak{I}(I). \tag{5}$$

Using Eqs. (3), (4), and (5), the angular velocity ω is eliminated and the following equations are obtained which determine the moment of inertia